VOL. 11 NO. 5,
FEBRUARY, 2026
E-ISSN 3027-1339
P-ISSN 3026-8257

African Scholar Publications & Research International
www.africanscholarpub.com

Journal of Systematic, Evaluation and Diversity Engr. (JSEDE)

Efficiency and Stability Optimization of Methyl Ammonium Lead Halide Perovskite: A Future Photovoltaic Solar Power for Mass Production

Mohammed Buba[1]; M.U. Abba[2]; Aaron Auliura Dengwaran[3]

[1]Department of Science Laboratory Technology Federal Polytechnic Mubi. [2]Department of Agricultural and Bio-environmental Engineering Technology. Federal Polytechnic Mubi. [3]Department of Physics School of Science Adamawa State College of education Hong

DOI: https://doi.org/10.70382/ajsede.v11i5.028

Abstract

Despite the rapid progress achieved in stability optimization of methylammonium lead iodide ($CH_3NH_3PbI_3$, $MAPbI_3$)–based perovskite solar cells (PSCs), further enhancement of device efficiency and operational stability remains a critical challenge, particularly through the optimization of charge transport layers. In this work, Ag–In co-doped SnO_2 thin films were synthesized via a cost-effective spray pyrolysis deposition technique and systematically investigated as electron transport layers (ETLs) for planar $MAPbI_3$ PSCs. The influence of silver doping concentration on the structural, optical, and electrical properties of SnO_2 was experimentally examined using Hall effect and UV–Vis spectroscopy measurements. The optimized SnO_2:Ag–In film, containing 3% Ag and 2% In, exhibited a low sheet resistance of 14.2 Ω sq^{-1}, high average optical transmittance of 92.39% in the visible range, and an enhanced optoelectronic figure of merit, indicating an excellent balance between conductivity and transparency.To establish a direct correlation between ETL material properties and device performance, experimentally extracted parameters were incorporated into SCAPS-1D numerical simulations. The optimized device architecture (FTO/Ag–In:SnO_2/$MAPbI_3$/Cu_2O/Au) achieved a remarkable power conversion efficiency of 31.82%, with an open-circuit voltage of 1.2868 V, a short-circuit

current density of 27.42 mA cm^{-2}, and a fill factor of 90.18%. A comprehensive parametric analysis was further conducted to evaluate the effects of absorber layer thickness, acceptor doping concentration, and defect density on device performance, leading to the identification of optimal design conditions for maximum efficiency. The results reveal that reduced defect density, optimized absorber thickness, and appropriate doping levels significantly suppress recombination losses and enhance charge extraction. Overall, this integrated experimental–simulation study demonstrates that Ag–In co-doped SnO_2 is a highly promising ETL for next-generation high-efficiency perovskite solar cells. The findings provide valuable insights into the rational design and optimization of charge transport layers, offering a viable pathway toward improved performance and stability in lead-based PSC technologies.

Keywords: Perovskite solar cells; Ag–In co-doped SnO_2; Electron transport layer; Spray pyrolysis; SCAPS-1D simulation; Device optimization

Introduction

Global interest within the solar cell (SC) research community in improving the performance of perovskite solar cells (PSCs) has led to a remarkable increase in their power conversion efficiency (PCE). Since their initial reported efficiency of 3.8% in 2009 [1], PSCs have rapidly progressed to 22.1% in 2017 [2] and are projected to reach 25.7% by 2023 [3]. This growing interest is driven by the continuous rise in global energy demand resulting from increased per capita energy consumption and rapid economic expansion.

Third-generation solar cells that employ organic–inorganic halide perovskites as light absorbers have attracted considerable attention due to their high performance and low production cost [4]. These materials exhibit exceptional optoelectrical properties, including tunable band gaps, long electron and hole diffusion lengths, low exciton binding energy, high defect tolerance, and excellent bipolar charge transport capabilities [5]. In addition, their chemical flexibility enables molecular engineering of the perovskite components, offering further opportunities for performance optimization [6].

Despite these advantages, perovskite absorber layers—typically methylammonium lead iodide ($CH_3NH_3PbI_3$ or $MAPbI_3$)—suffer from intrinsic and extrinsic defects that can negatively affect device performance. These defects may induce hysteresis [7], non-radiative recombination [8], charge trapping [9], charge scattering [10], and ion migration [11], ultimately limiting device stability and efficiency. Hybrid perovskites possess a crystal structure described by the general formula AMX_3 [12], where X represents a halide anion (Cl^-, Br^-, or I^-), M denotes a divalent metal cation such as Pb^{2+}, Sn^{2+}, or Ge^{2+}, and A is a small organic cation,

including $CH_3NH_3^+$, $CH_2(NH_2)_2^+$, or $C_2H_5NH_3^+$ [13].

The basic planar n–i–p architecture of PSCs comprises several functional layers: a transparent conducting oxide (TCO), an electron transport layer (ETL), the perovskite absorber layer ($MAPbI_3$), a hole transport layer (HTL), and a metallic back contact [14]. Each layer plays a crucial role in determining the overall efficiency and stability of the device. High-efficiency laboratory-scale PSCs commonly employ organic HTLs such as Spiro-MeOTAD, P3HT, PTAA, and PEDOT:PSS, as well as inorganic HTLs including NiO, CuI, Cu_2O, and CuSCN. A wide range of ETLs has also been investigated, including TiO_2, SnO_2, ZnO, PCBM, WO_3, ZnSe, CdZnS, C_{60}, IGZO, CdS, and others [15].

To minimize charge carrier recombination, the HTL should exhibit high carrier mobility and form a high-quality interface with the perovskite absorber layer [16]. Titanium dioxide (TiO_2) is one of the most widely used ETLs in PSCs due to its favorable electronic properties; however, its application is hindered by issues such as ion migration, ultraviolet (UV)-induced instability, and rapid performance degradation under UV exposure [17]. Consequently, alternative metal oxides such as zinc oxide (ZnO) and tin dioxide (SnO_2) have been extensively explored as substitutes for TiO_2 [18].

In this work, we investigate the optoelectrical properties of Ag–In co-doped SnO_2 thin films deposited using the spray pyrolysis technique, a simple and cost-effective fabrication method. The performance of Ag–In:SnO_2 as an ETL is systematically evaluated and compared with commonly used ETL materials, including TiO_2, PCBM, CdZnS, ZnO, ZnSe, IGZO, C_{60}, WO_3, and CdS. Methylammonium lead iodide ($MAPbI_3$) is employed as the absorber layer, while cuprous oxide (Cu_2O) is used as the HTL. Fluorine-doped tin oxide (FTO) is selected as the TCO due to its chemical inertness, thermal stability, mechanical robustness, high electrical conductivity, lower cost, and stable sheet resistance during high-temperature processing, in contrast to indium tin oxide (ITO), which exhibits increased resistance during sintering [19]. Device performance and optimization are analyzed using the SCAPS-1D software, a one-dimensional solar cell capacitance simulation tool.

Problem Statement

Despite the rapid advancement in perovskite solar cell (PSC) technology, achieving high efficiency together with long-term operational stability remains a major challenge. Methylammonium lead iodide ($MAPbI_3$)–based PSCs suffer from intrinsic and extrinsic defects that cause non-radiative recombination, charge trapping, ion migration, and performance degradation. Additionally, conventional electron transport layers (ETLs), particularly TiO_2, exhibit limitations such as ultraviolet-induced instability and reduced durability under operating conditions. These challenges hinder the large-scale commercialization of PSCs. Therefore, there is a need to explore alternative ETL materials with improved optoelectronic properties and to optimize key device parameters—such as absorber thickness, doping concentration, and defect density—to enhance both efficiency and stability of $MAPbI_3$-based solar cells.

Objectives of the Study

1. To synthesize and characterize Ag–In co-doped SnO_2 thin films and evaluate their optoelectrical properties as potential electron transport layers.
2. To investigate the performance of $MAPbI_3$-based perovskite solar cells incorporating the co-doped SnO_2 ETL using numerical simulation (SCAPS-1D).
3. To determine the optimal device parameters—including absorber thickness, doping concentration, and defect density—for maximizing photovoltaic performance.

Research Questions

1. How do Ag–In co-doped SnO_2 thin films perform as electron transport layers in $MAPbI_3$-based perovskite solar cells?
2. What is the effect of incorporating Ag–In co-doped SnO_2 on the efficiency and stability of the PSC device compared with conventional ETLs?
3. What are the optimal absorber-layer parameters (thickness, doping concentration, and defect density) required to achieve maximum device performance?

Experimental Procedures

Spray pyrolysis deposition (SPD) was selected as the thin-film fabrication technique due to its simplicity, cost-effectiveness, and ability to produce uniform, large-area oxide films with well-controlled stoichiometry. Ag–In co-doped SnO_2 thin films were deposited on thoroughly cleaned glass substrates with dimensions of 1×1.5 cm² using the SPD method. In this technique, a precursor solution is atomized and sprayed onto a heated substrate, where thermal decomposition and chemical reactions lead to the formation of the thin film.

The precursor solutions were prepared using tin(IV) chloride pentahydrate ($SnCl_4 \cdot 5H_2O$, 99.99%, Alfa Aesar) as the tin source, with indium chloride ($InCl_3$, 99.99%, Alfa Aesar) and silver nitrate ($AgNO_3$, 99.99%, Alfa Aesar) serving as dopant precursors. These chemicals were dissolved at appropriate concentrations in ethanol (C_2H_5OH, 99.99%, Alfa Aesar). The resulting solution was atomized using argon as the carrier gas and directed onto the heated substrates to form co-doped SnO_2 thin films.

The uniformity and surface morphology of the deposited Ag–In:SnO_2 layers were strongly influenced by several deposition parameters, including substrate temperature, precursor flow rate, spray rate, and nozzle-to-substrate distance. In this study, the substrate temperature was maintained at approximately 450 °C to ensure sufficient thermal decomposition of the precursors and to enhance film crystallinity while preventing film cracking. The atomization rate and carrier gas flow were optimized to achieve fine aerosol formation and uniform droplet distribution across the substrate surface. The nozzle-to-substrate distance was kept constant to control film thickness and minimize shadowing effects.

Electrical characterization of the films was carried out using an ECOPIA HMS-1000 Hall measurement system operating in the van der Pauw configuration. This technique enabled

precise determination of key electrical parameters, including charge carrier concentration, carrier mobility (μ), electrical conductivity (σ), and resistivity (ρ).

The Hall effect, which describes the development of a transverse voltage in a current-carrying conductor subjected to a magnetic field, was utilized to evaluate charge transport properties. In the van der Pauw method, which is suitable for nearly square and uniform samples, current is applied between diagonally opposite contacts while a magnetic field is applied perpendicular to the sample surface. The Hall coefficient is then determined from the voltage measured across the remaining two contacts, both in the presence and absence of the magnetic field. The Hall coefficient is directly related to the charge carrier concentration and mobility.

Four electrical probes were mounted on the surface of a ceramic sample holder and connected to coaxial cables from the underside of the holder. The probes were centrally hinged, allowing precise adjustment for measurements on samples with an effective square area of 8 mm × 8 mm. A magnetic field strength of 0.56 Tesla was applied during the measurements. Film thickness was determined using a mechanical profilometer.

Optical characterization was performed using a PerkinElmer Lambda 950 UV–Vis–NIR spectrophotometer operated at a scanning rate of 0.1 nm s^{-1} to obtain the optical transmittance and absorption spectra of the thin films.

Simulation Framework

The solar cell (SC) modeling tool used in this study was SCAPS-1D, a numerical simulation software developed by the Department of Electronics and Information Systems at the University of Ghent, Belgium [21]. All device structures discussed in the subsequent sections were designed and simulated using this software. SCAPS-1D employs numerical differentiation in combination with Gummel's iterative method to solve the Poisson equation and the continuity equations for charge carriers, namely electrons and holes [22]. Once the operating point is determined, the software generates key photovoltaic parameters, including current density, electric potential, power conversion efficiency, and fill factor.

A series of perovskite solar cell structures were proposed and computationally designed under standard operating conditions using the AM 1.5G solar spectrum at a temperature of 300 K and an incident light intensity of 1000 W m^{-2}. To investigate the influence of the electron transport layer (ETL) on device performance, a comparative analysis was conducted between Ag–In co-doped SnO_2–based structures and several commonly used organic and inorganic ETL materials.

The simulated device architecture consisted of fluorine-doped tin oxide (FTO) as the anode, methylammonium lead iodide ($MAPbI_3$) as the active absorber layer, and cuprous oxide (Cu_2O) as the hole transport layer (HTL). The ETL materials considered in this study included Ag–In:SnO_2, TiO_2, PCBM, CdZnS, ZnO, ZnSe, IGZO, C_{60}, WO_3, and CdS. A schematic illustration of the simulation framework is presented in Fig. 1, while the detailed input parameters used for the device simulations are summarized in Table 1.

The electron and hole thermal velocities were set to 10^7 cm s^{-1}. The work functions of the front and back contacts were defined as 4.4 eV for FTO and 5.1 eV for the gold (Au) back contact, respectively. To more accurately represent interfacial recombination effects, interface defect layers (IDLs) were introduced at the ETL/$MAPbI_3$ and $MAPbI_3$/HTL interfaces. The parameters associated with these interface defect layers are provided in Table 1.

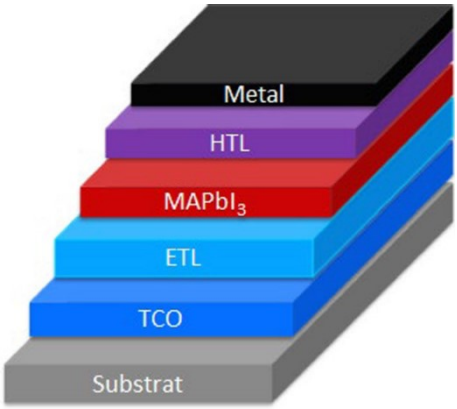


Figure 1 FTO/ETL/MAPbI3/Cu2O/Au

Table 1 The defect parameters of various layers of the simulated device [12]

Parameters	FTO	ETL	MAPbI3	Cu2O	MAPbI3/HTM	ETL/MAPbI3
Type	Neutral	Neutral	Neutral	Neutral	acceptor	acceptor
defect density Nt (cm^{-3})	1015	–	1016	1014	10^9	10^9
Capture cross section electrons (cm^2)	10–15	10–15	10–15	10–15	10–18	10–19
Capture cross section holes (cm^2)	10–15	10–15	10–15	10–15	10–19	10–20
Reference for defect energy level Et	Above EV	Above EV	Above EV	Above EV	Above highest EV	Above highest EV
Energy level with respect to reference	0.6	0.6	0.6	0.6	0.32	0.07

Table 2 Average transmissions values of SnO_2:Ag-In films and their maxima

0	**3.55**	**97.97**	**96.62**	**99.56**	**782.1**
1	3.41	96.96	96.25	99.04	795.0
2	3.39	94.10	93.69	97.03	675.7
3	3.32	92.39	92.20	94.51	790.3
4	3.29	90.25	90.54	93.29	862.0
8	3.16	85.68	85.95	89.97	772.1
12	3.05	81.57	81.30	85.34	744.5

Optical Study

The average transmittance (T_avg) of the SnO_2:Ag–In thin films, evaluated in the visible region (400–800 nm) as well as over the entire measured optical range (350–1000 nm), is summarized in Table 2. The table also presents the maximum transmittance values and their corresponding wavelengths for different silver doping concentrations. Figure 2 illustrates the variation of optical transmittance of the SnO_2:Ag–In films as a function of wavelength.

For all samples, the transmittance reaches its maximum within the visible region, specifically between 675 and 862 nm. The maximum transmittance decreases monotonically with increasing silver doping concentration, from 97.97% for the undoped sample to 81.57% for the sample doped with 12% Ag.

The absorption coefficient, α (cm^{-1}), was calculated from the measured transmittance data using the relation

$$\alpha = (1/d)\ln(1/T) = (2.303/d)\log10(1/T) \quad \ldots\ldots 1$$

where d is the film thickness (cm), T is the transmission coefficient, and R is the reflection coefficient (in %) [15].

The UV–Vis absorption spectra were further used to determine the optical band gap of the films. According to the literature, the investigated compounds exhibit a direct allowed transition. Therefore, the optical band gap was evaluated using the Tauc relation:

$$(\alpha h\nu)^2 = A(h\nu - E_g) \quad \ldots\ldots 2$$

where α is the absorption coefficient (cm^{-1}), hν is the photon energy (eV), A is a material-dependent constant, and E_g is the optical band gap energy (eV).

By plotting $(\alpha h\nu)^2$ as a function of photon energy hν and extrapolating the linear portion of the curve to intersect the photon-energy (abscissa) axis, the optical band gap E_g was determined (see Fig. 3).

The results show that increasing the Ag concentration leads to a reduction in the optical band gap, decreasing from 3.55 eV for the undoped film to 3.05 eV for the film with the highest Ag content.

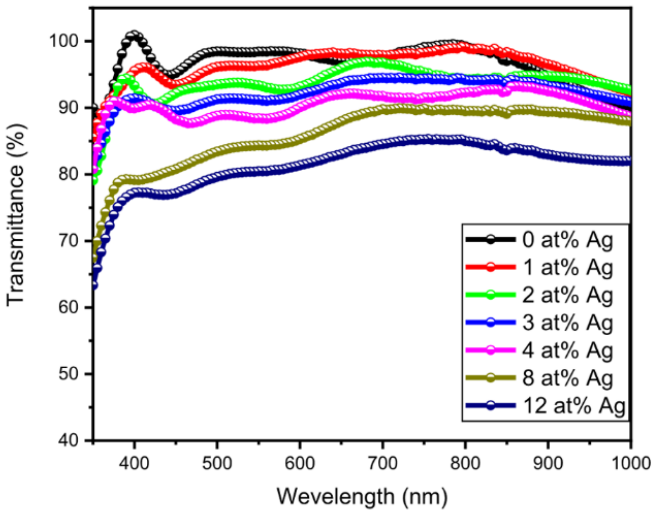


Fig. 2 Optical transmittance of SnO_2:In-Ag thin films of different Ag doping concentration

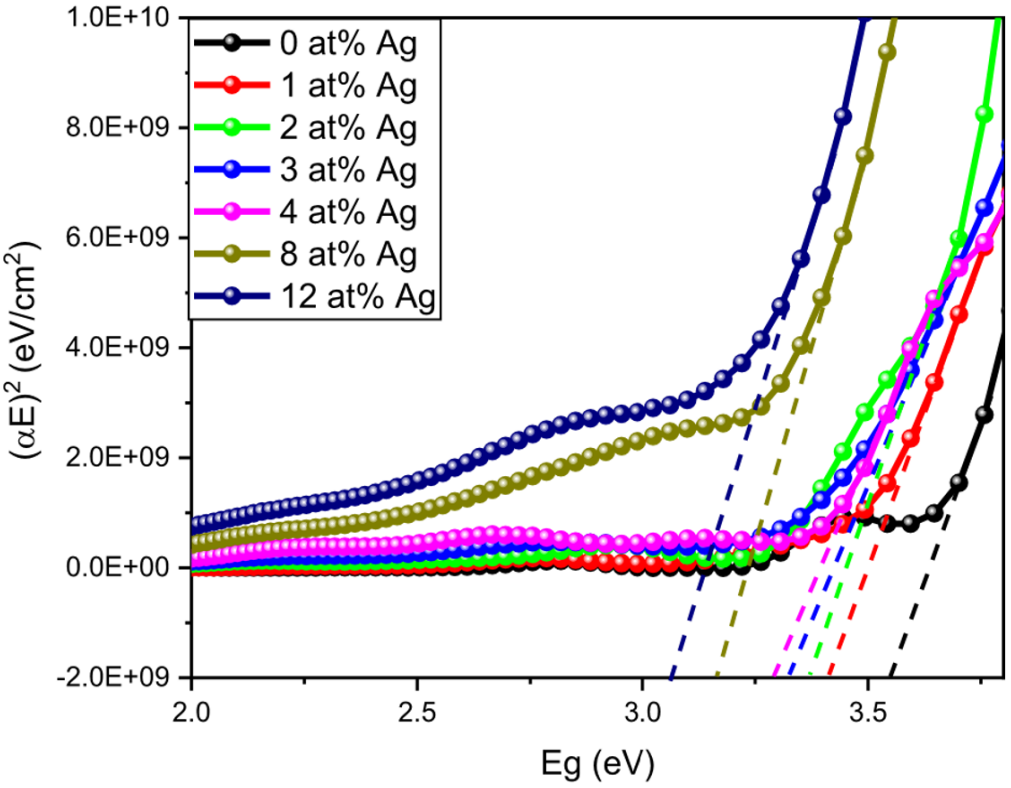


Fig. 3 Optical transmittance of SnO_2:In-Ag thin films of different Ag doping concentration

Electrical study

The electrical properties of SnO_2:Ag–In thin films were investigated as a function of silver doping concentration using Hall effect measurements in a four-point coplanar configuration. The electrical parameters obtained for the SnO_2:Ag–In films are summarized in Table 4. The results show that the electrical resistivity decreases progressively with increasing Ag doping at low concentrations. A sheet resistance of 27.3 Ω sq^{-1} was measured for the undoped SnO_2 film, which gradually decreased with the incorporation of small amounts of silver, reaching a minimum value of 11.9 ± 0.7 Ω sq^{-1} for films doped with 4% Ag.

This reduction in resistivity indicates that, at low doping levels, silver is uniformly incorporated into the SnO_2 lattice and acts as an effective dopant by increasing the charge carrier concentration, thereby enhancing the electrical conductivity of the films. However, at higher doping concentrations (8–12%), the electrical resistivity of the co-doped SnO_2 films increases again, reaching approximately 24.8 Ω sq^{-1} for films containing 12% Ag. This increase may be attributed to the segregation of silver and its subsequent oxidation, which can disrupt charge transport pathways and introduce trap states that hinder carrier conduction [23].

The figure of merit is an important parameter for evaluating the overall optoelectronic performance of the films, as it reflects the balance between electrical conductivity and optical transparency.

Table 4 Electrical parameters obtained for deposited SnO2:Ag-In thin films

Ag doping(%)	Thickness (nm)	ρ (10^{-4} Ω.cm)	R sq (Ω/sq)	Φ_{TC} 10^{-2} Ω^{-1}
0	132	3.6 ± 0.14	27.3 ± 1.06	2.99 ± 0.11
1	140	2.4 ± 0.15	17.1 ± 1	4.29 ± 0.26
2	141	2.3 ± 0.14	16.3 ± 0.98	3.34 ± 0.2
3	141	2.0 ± 0.12	14.2 ± 0.85	3.20 ± 0.19
4	143	1.7 ± 0.1	11.9 ± 0.7	3.02 ± 0.17
8	143	2.1 ± 0.14	14.7 ± 0.92	1.45 ± 0.09
12	145	3.6 ± 0.15	24.8 ± 1.03	0.56 ± 0.02

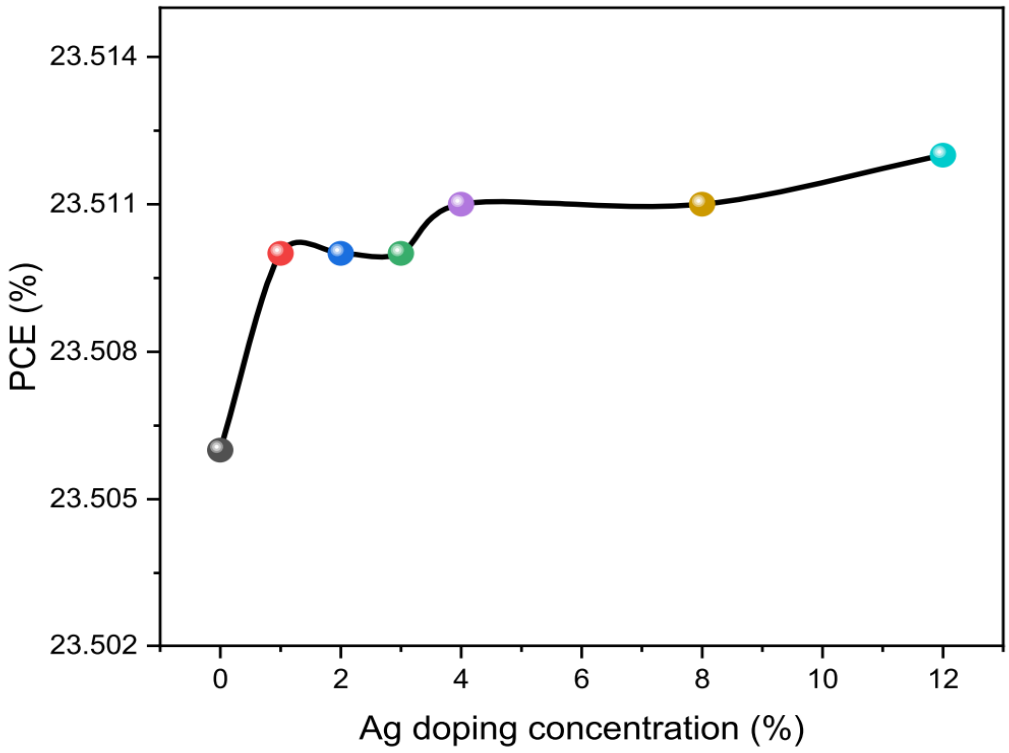


Fig. 4 Influence of increasing Ag concentration in ETL on PCE

Figure 4 illustrates the influence of increasing silver concentration in the electron transport layer (ETL) on the power conversion efficiency (PCE) reliability of transparent electrodes, highlighting the trade-off between electrical conductivity and optical transparency. The figure of merit, which serves as a key parameter for evaluating the optoelectrical performance of transparent conducting films, was determined using the method proposed by G. Haacke [24]. The figure of merit reaches its maximum values for SnO_2:Ag–In films doped with 3% and 4% Ag, with values of $(3.20 \pm 0.19) \times 10^{-2}$ and $(3.02 \pm 0.17) \times 10^{-2}$, respectively. For Ag doping concentrations below 3%, the figure of merit remains relatively high, indicating a favorable balance between optical transmittance and electrical conductivity. However, at higher doping

levels, the figure of merit decreases due to the degradation of optical transparency and increased carrier scattering

The figure of merit remains relatively high for low silver doping concentrations, varying from $(4.29 \pm 0.26) \times 10^{-2}$ to $(2.99 \pm 0.11) \times 10^{-2}$. However, it decreases significantly at higher doping levels (8–12%), reaching values as low as approximately $(0.56 \pm \ldots) \times 10^{-2}$. This decline is attributed to the deterioration of optoelectrical properties caused by excessive silver incorporation.

Based on the optoelectrical analysis, it can be concluded that an Ag doping concentration of 3% represents the optimal condition for achieving SnO_2:Ag–In thin films with a favorable balance between high optical transparency and low electrical resistivity.

Comparison of Different ETLs and Their Performance

The proposed perovskite solar cell was designed using a planar n–i–p architecture with the configuration Glass/FTO/ETL/$MAPbI_3$/Cu_2O/Au to investigate the influence of different electron transport layers (ETLs) on key photovoltaic performance parameters, including the fill factor (FF), open-circuit voltage (V_OC), short-circuit current density (J_SC), and power conversion efficiency (PCE). In particular, the effects of varying band gaps associated with SnO_2:Ag–In films and other commonly used ETLs were systematically examined.

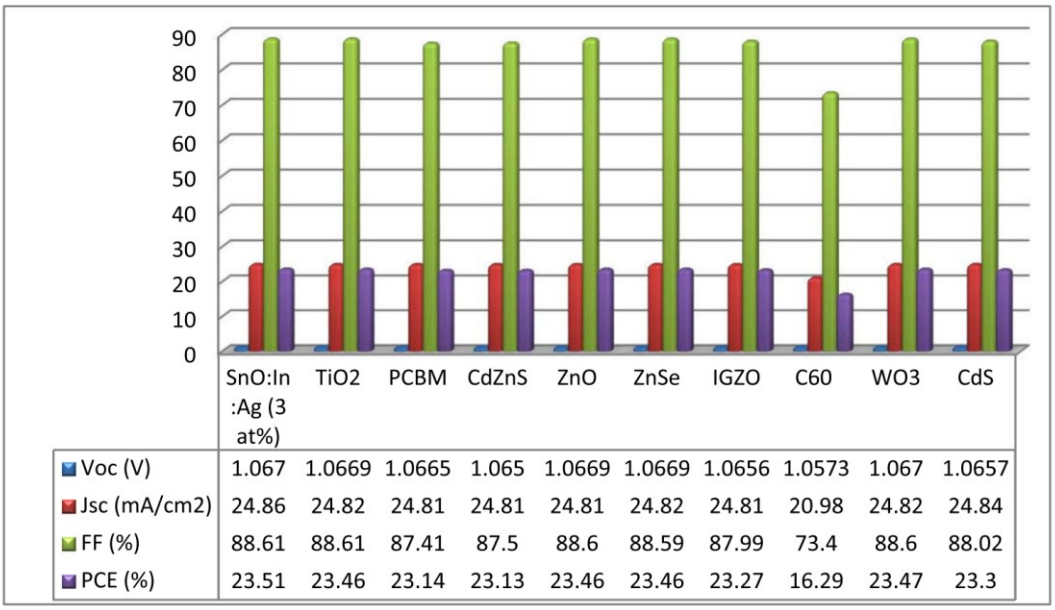
The experimentally determined thicknesses and band gap values of the SnO_2:Ag–In films were incorporated into the SCAPS-1D simulations to evaluate their impact on device performance. As shown in Fig. 4, the PCE exhibits slight variation with increasing silver concentration in the ETL, reaching 23.55% for the device incorporating 3% Ag-doped SnO_2. Figure 5 presents the photovoltaic parameters used in the simulations.

A total of ten device structures were analyzed, each with uniform layer thicknesses of 500 nm for the FTO electrode, 141 nm for the ETLs (SnO_2:Ag–In (3%), TiO_2, PCBM, CdZnS, ZnO, ZnSe, IGZO, C_{60}, WO_3, and CdS), 450 nm for the $MAPbI_3$ absorber layer, and 200 nm for both the Cu_2O hole transport layer and the Au back contact. For consistency, a uniform shallow donor density (N_D) of 1×10^{17} cm^{-3} was assigned to all ETLs.

Among the ETLs investigated, the device employing SnO_2:Ag–In (3%) demonstrated the best overall performance, achieving a fill factor of 88.61% and a power conversion efficiency of 23.51%. The simulated current–voltage (J–V) characteristics of the devices are shown in Fig. 6. Notably, the SnO_2:Ag–In (3%)-based device delivered the highest short-circuit current density (J_SC) of 24.86 mA cm^{-2} and an open-circuit voltage (V_OC) of 1.0670 V. This enhanced performance can be attributed to favorable energy band alignment at the ETL/$MAPbI_3$ interface, which promotes efficient charge extraction and suppresses recombination losses.

Furthermore, the SnO_2:Ag–In (3%)-based perovskite solar cell exhibited high photon absorption efficiency, contributing to the observed increase in current density. Based on these results, SnO_2:Ag–In (3%) was selected as the optimal ETL for the second phase of this study. A detailed analysis was subsequently conducted to investigate the effects of absorber layer

properties—including $MAPbI_3$ thickness, donor density, and defect density—on the overall device performance.



	SnO:In :Ag (3 at%)	TiO2	PCBM	CdZnS	ZnO	ZnSe	IGZO	C60	WO3	CdS
Voc (V)	1.067	1.0669	1.0665	1.065	1.0669	1.0669	1.0656	1.0573	1.067	1.0657
Jsc (mA/cm2)	24.86	24.82	24.81	24.81	24.81	24.82	24.81	20.98	24.82	24.84
FF (%)	88.61	88.61	87.41	87.5	88.6	88.59	87.99	73.4	88.6	88.02
PCE (%)	23.51	23.46	23.14	23.13	23.46	23.46	23.27	16.29	23.47	23.3

Fig. 5 Device performance parameters by varying ETMs with perovskite thickness set as 450 nm

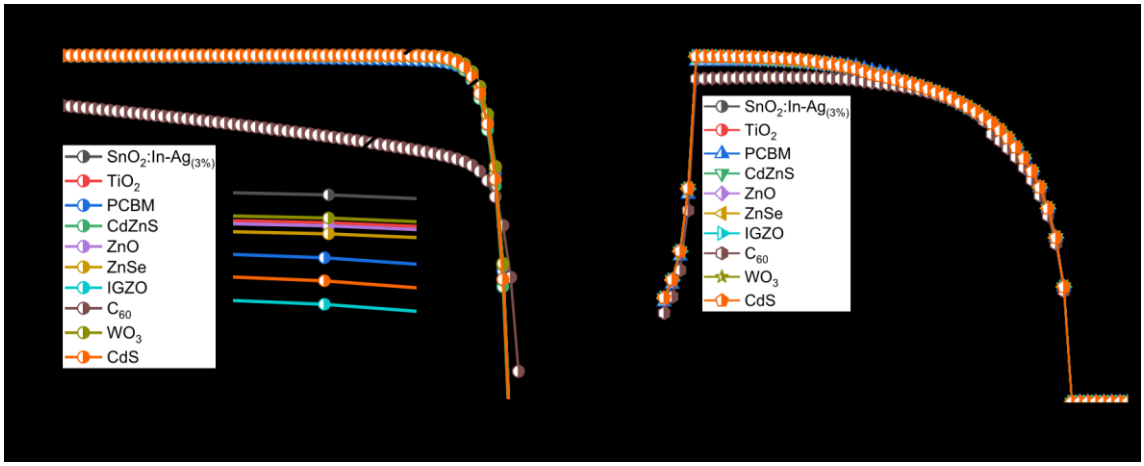


Fig. 6 Influence of different ETM candidates on the $MAPbI_3$-based solar cell performance using Cu_2O as HTM (**a**) J-V characteristics, (**b**) quantum efficiency

Effect of the Absorber Layer Thickness

The thickness of the active absorber layer is one of the most critical parameters influencing the performance of perovskite solar cells, as it directly affects the propagation length and lifetime of photogenerated charge carriers (electrons and holes) [23]. Therefore, careful optimization of the absorber thickness is essential to achieve high device efficiency.

Figure 7 presents the quantum efficiency (QE) spectra and the current–voltage (J–V) characteristics for absorber thicknesses ranging from 100 to 2000 nm. Both the external quantum efficiency (EQE) and internal quantum efficiency (IQE) were considered in evaluating device performance. The EQE is defined as the ratio of the number of charge carriers generated in the absorber to the number of incident photons, whereas the IQE represents the ratio of collected charge carriers contributing to the photocurrent to the number of absorbed photons at a given wavelength [24].

Increasing the absorber thickness enhances photon absorption within the $MAPbI_3$ layer, leading to a higher generation rate of photoexcited charge carriers. This improvement positively influences the quantum efficiency and results in an increase in the short-circuit current density (J_{SC}). However, excessive absorber thickness increases the probability of charge carrier recombination, particularly when the carrier diffusion length becomes shorter than the absorber thickness, as illustrated in Fig. 7a. Under such conditions, a significant fraction of photogenerated carriers recombine before reaching the charge-collecting contacts, thereby degrading device performance [25].

Further increases in the thickness of the $MAPbI_3$ absorber layer lead to a continuous rise in quantum efficiency, reaching a near-saturation maximum value of approximately 99.9%, as shown in Fig. 7b. This high QE indicates efficient generation of electron–hole pairs within the absorber. To explain the slight variation observed in the open-circuit voltage (V_oc), an analytical approximation based on the single-diode model can be applied [26]:

$$V_{OC} = (n\ k\ T / q) \ln(J_{SC} / J_0 + 1)$$

where n is the diode ideality factor, k is Boltzmann's constant, T is the absolute temperature, q is the elementary charge, and J_0 is the reverse saturation current density.

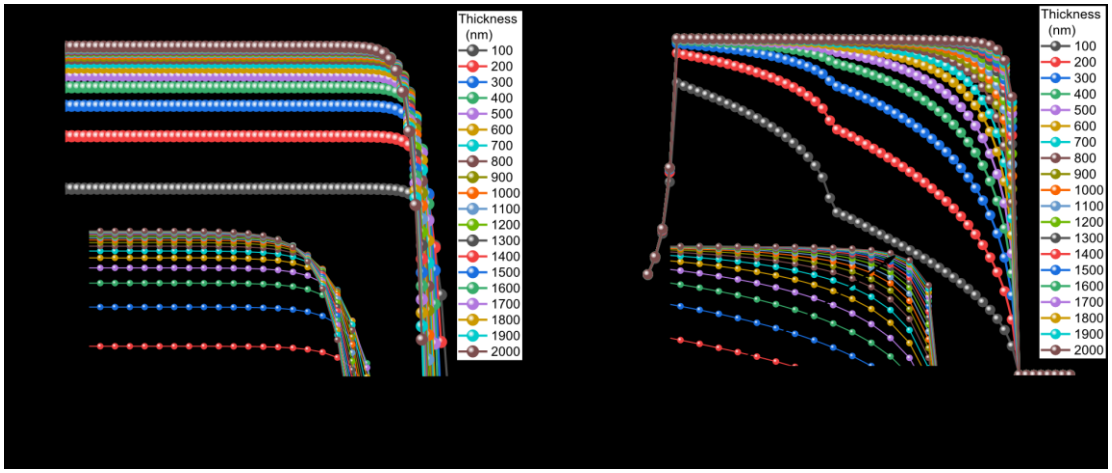
The term nkT/q represents the thermal voltage.

The influence of absorber thickness on the short-circuit current density (J_{SC}) is illustrated in Fig. 8. As the absorber thickness increases, J_{SC} rises from 13.94 mA cm^{-2} to a maximum value of 28.15 mA cm^{-2}, which approximately corresponds to the carrier diffusion length. Beyond this thickness, J_{SC} enters a saturation regime, indicating that additional absorber material no longer contributes significantly to photocurrent generation.

In contrast, increasing the absorber thickness adversely affects both the open-circuit voltage (V_{OC}) and the fill factor (FF). Specifically, V_{OC} decreases from 1.0901 V to 1.0320 V, while the FF declines from 75.79% to 69.04%. This behavior is attributed to enhanced charge carrier recombination [27] and an increase in the reverse saturation current density J_0 [28], as described by Eq. (4).

Despite the reductions in V_{OC} and FF, the improved light absorption associated with increased absorber thickness leads to an overall enhancement in the power conversion efficiency (PCE). The PCE reaches a maximum value of 25.48% at an absorber thickness of 900 nm. Beyond this point, the PCE remains nearly constant up to approximately 1700 nm, after which a gradual decline is observed.

Considering both device performance and the increased material consumption and fabrication costs associated with thicker absorber layers, an optimal $MAPbI_3$ thickness of 900 nm is selected for subsequent simulations. At this optimized thickness, the device exhibits a V_{OC} of 1.0516 V, a J_{SC} of 27.39 mA cm^{-2}, a fill factor of 88.46%, and a PCE of 25.48%.



Effect of Absorber Doping Concentration (N_a)

The doping density is a key parameter governing the electrical properties of the individual layers in a solar cell, as it determines their p-type or n-type behavior and strongly influences charge transport and recombination processes. By controlling the doping level, the electrical conductivity of the absorber can be effectively tuned, thereby impacting overall device performance.

In this study, the effect of varying the acceptor doping concentration (N_a) of the $MAPbI_3$ absorber layer was investigated over the range from 1×10131 \times 10^{13}1×1013 to 5×1021 cm−35 \times 10^{21}\,\text{cm}^{-3}5×1021cm−3, while maintaining the previously optimized layer thicknesses. Figure 9 illustrates the dependence of the photovoltaic parameters on the absorber doping concentration.

The values of V_oc, J_sc, FF, and PCE remain relatively stable up to an acceptor concentration of 1×1016 cm−31 \times 10^{16}\,\text{cm}^{-3}1×1016cm−3. Beyond this threshold, a pronounced enhancement in device performance is observed as the doping level increases. Most parameters continue to improve up to a concentration of 1×1021 cm−31 \times 10^{21}\,\text{cm}^{-3}1×1021cm−3, with the exception of J_sc, which exhibits a slight reduction at very high doping levels.

This behavior can be attributed to a decrease in the reverse saturation current density (J_0), leading to enhanced V_oc and FF, as described by Eq. (4). As shown in Fig. 9, the maximum power conversion efficiency is achieved at high absorber doping concentrations, indicating improved carrier collection and reduced recombination losses.

To ensure both high performance and device stability, an acceptor doping concentration of 1×1020 cm−31 \times 10^{20}\,\text{cm}^{-3}1×1020cm−3 was selected for subsequent

simulations. Under these optimized conditions, the solar cell exhibits a V_oc of 1.1707 V, a J_sc of 27.36 mA cm^{-2}, a fill factor of 89.43%, and a power conversion efficiency of 28.65%.

Effect of Absorber Defect Density (N_t)

In addition to absorber thickness and acceptor doping concentration, the total defect density (N_t) within the perovskite absorber layer plays a critical role in determining the performance and stability of perovskite solar cells (PSCs). An increased defect density enhances nonradiative recombination, promotes pinhole formation, accelerates film degradation, and ultimately degrades device efficiency and operational stability [29]. Consequently, PSCs with high defect densities typically exhibit reduced carrier lifetimes and inferior photovoltaic performance.

To evaluate the influence of absorber defect density on device characteristics, simulations were conducted by varying N_t from 1×10121 \times 10^{12}1×1012 to 1×1017 cm−31 \times 10^{17}\,\text{cm}^{-3}1×1017cm−3. The resulting current–voltage (J–V) characteristics for different defect densities are presented in Fig. 10, while Fig. 11 illustrates the corresponding evolution of key photovoltaic parameters.

As the defect density increases, a systematic degradation in overall device performance is observed. This decline manifests as reductions in V_oc, J_sc, fill factor (FF), and power conversion efficiency (PCE). The observed trend is primarily attributed to enhanced Shockley–Read–Hall (SRH) recombination, which becomes more pronounced at higher defect concentrations and limits effective charge carrier transport and collection within the absorber layer

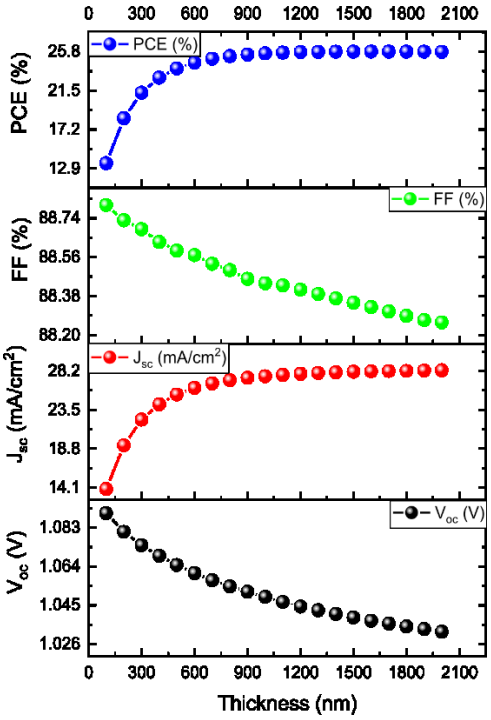


Fig. 8 Variation of device performance with absorber thickness

It is observed that J_sc, FF, and PCE exhibit only a slight reduction as the defect density increases up to 1×10^{15} cm^{-3} . Beyond this threshold, all three parameters decrease rapidly with further increases in defect density. The reduction in J_sc can be attributed to defect-assisted charge carrier recombination, which in turn leads to a decline in the fill factor due to the increased series resistance of the device [30]. As the defect density increases, the open-circuit voltage (V_oc) decreases significantly, dropping from 1.2868 V to 1.0061 V, indicating a strong sensitivity of V_oc to defect-related recombination processes.

The overall deterioration in device performance is primarily associated with the increased density of defect states, which act as trapping centers and create additional nonradiative recombination pathways within the absorber layer [31]. Consequently, as the defect density rises, the power conversion efficiency decreases dramatically from 31.82% to 11.71%. This efficiency loss is mainly due to the reduced charge carrier diffusion length and the enhanced recombination of photogenerated carriers within the perovskite absorber layer [32].

Comparison Between Experimental Data and Simulated Device Parameters

Considering all optimization stages, an optimal device configuration was achieved with an absorber thickness of 900 nm, an acceptor doping concentration of 1×10^{20} cm^{-3}, and a defect density of 1×10^{12} cm^{-3}. Under these conditions, the simulated perovskite solar cell exhibits the following performance parameters: an open-circuit voltage (V_{OC}) of 1.2868 V, a short-circuit current density (J_{SC}) of 27.42 $mA \cdot cm^{-2}$, a fill factor (FF) of 90.18%, and a power conversion efficiency (PCE) of 31.82%.

CONCLUSION

In this study, the performance of planar perovskite solar cells (PSCs) with a Glass/FTO/ETL/$MAPbI_3$/Cu_2O/Au configuration was systematically enhanced through comprehensive numerical optimization using the SCAPS-1D simulation platform. Experimentally obtained optoelectrical properties of Ag–In co-doped SnO_2 thin films were incorporated into the model to assess their effectiveness as electron transport layers (ETLs). The results demonstrate that Ag–In:SnO_2 is a highly promising ETL material, yielding superior device performance compared with several conventional ETLs due to its favorable band alignment, high conductivity, and excellent optical transparency.

A detailed parametric study revealed that the absorber layer thickness strongly influences photon absorption and carrier recombination. An optimal $MAPbI_3$ thickness of 900 nm was identified, providing a balance between efficient light harvesting and minimal recombination losses. Similarly, the acceptor doping concentration of the absorber was found to be a critical factor controlling carrier transport and device output. Increasing the doping density improved the built-in electric field and carrier collection efficiency, with an optimal value of 1×10^{20} cm^{-3} yielding the best performance.

The impact of defect density within the absorber layer was also examined, showing that increased defect concentrations significantly degrade device performance due to enhanced Shockley–Read–Hall recombination and reduced carrier lifetimes. Low defect densities (~1×10^{12} cm^{-3}) were therefore essential for achieving high efficiency and operational stability.

Under the optimized conditions—absorber thickness of 900 nm, acceptor doping concentration of 1×10^{20} cm^{-3}, and defect density of 1×10^{12} cm^{-3}—the simulated PSC achieved outstanding performance metrics, including an open-circuit voltage (V_oc) of 1.2868 V, a short-circuit current density (J_sc) of 27.42 $mA \cdot cm^{-2}$, a fill factor of 90.18%, and a power

conversion efficiency (PCE) of 31.82%. These results highlight the strong potential of Ag–In co-doped SnO_2 as an efficient ETL for high-performance perovskite solar cells.

Overall, this work provides valuable insights into the interplay between material properties and device physics in PSCs and offers practical guidelines for the design and optimization of next-generation high-efficiency perovskite solar cells.

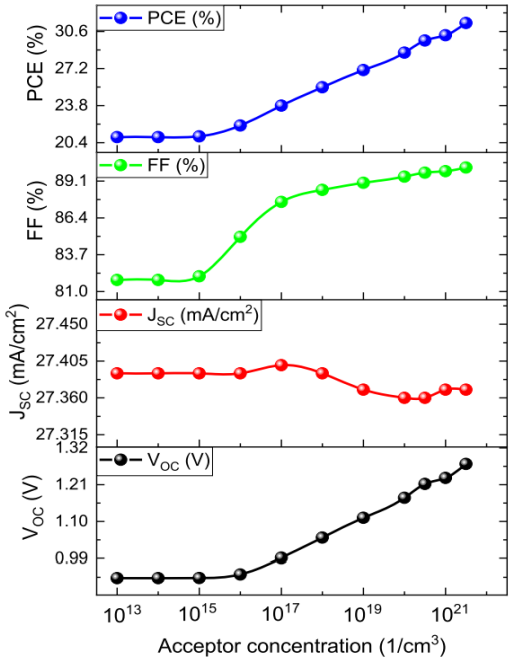


Fig. 9 Variation of device performance with acceptor doping concentration of the absorber

The simulation results clearly demonstrate that Ag–In co-doped SnO_2 is a highly promising ETL material, offering superior performance compared to commonly used alternatives such as TiO_2, ZnO, ZnSe, and WO_3 within the FTO/ETL/$MAPbI_3$/Cu_2O/Au configuration. Furthermore, a detailed parametric analysis was conducted to elucidate the influence of key absorber-layer properties—including thickness, acceptor doping concentration, and defect density—on overall device peformance.

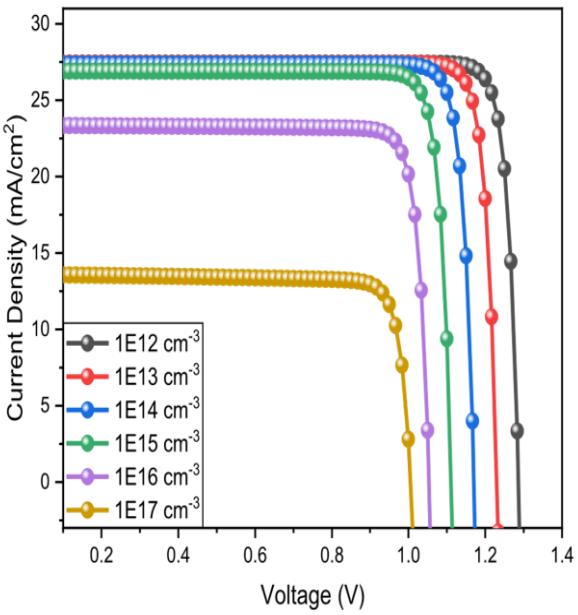


Fig. 10 J-V characteristics for perovskite absorber layer defect density

Overall, the integration of Ag–In co-doped SnO_2 as an ETL represents a promising design strategy for next-generation lead-based perovskite solar cells. This approach offers substantial potential for advancing device efficiency and provides valuable insights for the development of high-performance and scalable photovoltaic technologies.mA·cm^{-2}, and a fill factor of 90.18%. These findings underscore the critical role of absorber-layer optimization in maximizing PSC performance.

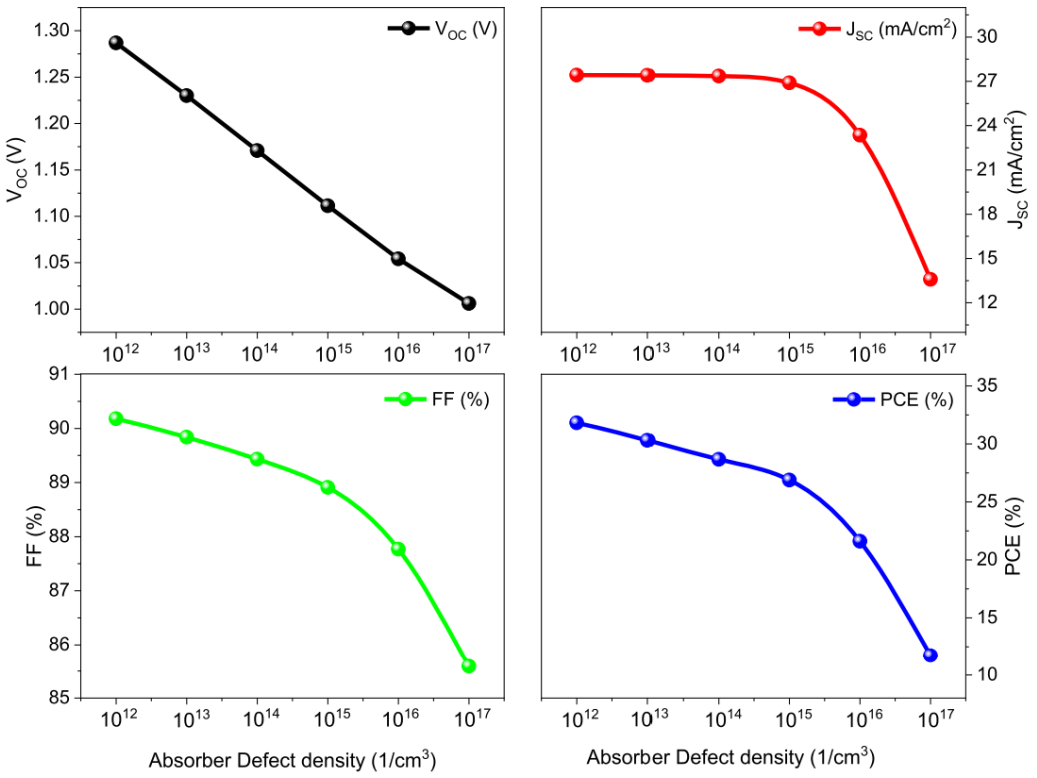


Fig. 11 Variation of device mperformance with absorber's layer defect density

Funding This work was supported by Tertiary Education trust Fund Intervention Nigeria (Tetfund) through Institutional Base Research programmer (IBR) 2025

Acknowledgement: The authors gratefully acknowledge the Tertiary Education Trust Fund (TETFund), Nigeria, for the financial support provided for this research. We also sincerely appreciate the management of the Federal Polyttechnic, Mubi, through the Directorate of Research and Innovation, for considering this research worthy of suppo

References

R. Jaiswal, R. Ranjan, N. Srivastava, A.K. Sharma, M. Yoshimura, L. Chang, R.N. Tiwari, Numerical study of eco-friendly Sn-based Perovskite solar cell with 25.48% efficiency using SCAPS-1D. J. Mater. Sci. Mater. Electron. **34**, 753 (2023). https://doi.org/10.1007/s10854-023-10171-w

M.K. Hossain, G.F.I. Toki, A. Kuddus, M.K.A. Mohammed, R. Pandey, J. Madan, S. Bhattarai, M.F. Rahman, D.K. Dwivedi, M. Amami, H. Bencherif, D.P. Samajdar, Optimization of the architecture of lead-free CsSnCl3-perovskite solar cells for enhancement of efficiency: a combination of SCAPS-1 D and wxAMPS study. Mater. Chem. Phys. **308**, 128281 (2023). https://doi.org/10.1016/j.matchemphys.2023.128281

Q. Duan, J. Ji, X. Hong, Y. Fu, C. Wang, K. Zhou, X. Liu, H. Yang, Z.-Y. Wang, Design of hole-transport-material free CH3NH3PbI3/CsSnI3 allperovskite heterojunction efficient solar cells by device simulation. Sol. Energy **201**, 555–560 (2020). https://doi.org/10.1016/j.solener.2020.03.037

S. Liu, V.P. Biju, Y. Qi, W. Chen, Z. Liu, Recent progress in the development of high-efficiency inverted perovskite solar cells. NPG Asia Mater. **15**, 1–28 (2023). https://doi.org/10.1038/s41427-023-00474-z

O. Daoudi, I. Jellal, A. Haddout, J. Zimou, O. EL Khouja, K. Nouneh, M. Lharch, M. Fahoume, A. Bendoumou, Unravelling the role of nickel incorporation on the physical properties of CuO thin films deposited by spray pyrolysis and theoretical analysis of nanostructured ZnO/Ni:CuO-based heterojunction solar cells. J. Mater. Sci. Mater. Electron. **34**, 819 (2023). https://doi.org/10.1007/s10854-023-10167-6

M. Saliba, T. Matsui, K. Domanski, J.-Y. Seo, A. Ummadisingu, S.M. Zakeeruddin, J.-P. Correa-Baena, W.R. Tress, A. Abate, A. Hagfeldt, M. Grätzel, Incorporation of rubidium cations into perovskite solar cells improves photovoltaic performance. Science **354**, 206–209 (2016). https://doi.org/10.1126/ science.aah5557

J.S. Manser, P.V. Kamat, Band filling with free charge carriers in organometal halide perovskites. Nat. Photon. **8**, 737–743 (2014). https://doi.org/10. 1038/nphoton.2014.171

H. Chen, F. Ye, W. Tang, J. He, M. Yin, Y. Wang, F. Xie, E. Bi, X. Yang, M. Grätzel, L. Han, A solvent- and vacuum-free route to large-area perovskite films for efficient solar modules. Nature **550**, 92–95 (2017). https://doi.org/10.1038/nature23877

S.E. Boussaada, Y. Mouchaal, H. Riane, A. Khelil, Performance enhancement of lead-free CsSnI3 and CsSnCl3 perovskite solar cells by tuning layer interfaces. Opt. Quant. Electron. **57**, 545 (2025). https://doi.org/10.1007/s11082-025-08461-0

M. Liu, M.B. Johnston, H.J. Snaith, Efficient planar heterojunction perovskite solar cells by vapour deposition, Nature 501 (2013) 395–398. https:// www.nature.com/articles/nature12509 (accessed January 21, 2024).

Z. Wang, Q. Lin, F.P. Chmiel, N. Sakai, L.M. Herz, H.J. Snaith, Efficient ambient-air-stable solar cells with 2D–3D heterostructured butylammoniumcaesium-formamidinium lead halide perovskites, Nature Energy 2 (2017) 1–10. https://www.nature.com/articles/nenergy2017135 (accessed January 21, 2024).

F. Ghamsari-Yazdel, I. Gharibshahian, S. Sharbati, Thin oxide buffer layers for avoiding leaks in CIGS solar cells; a theoretical analysis. J. Mater. Sci. Mater. Electron. **32**, 7598–7608 (2021). https://doi.org/10.1007/s10854-021-05476-7

S.E. Boussaada, Y. Mouchaal, H. Riane, A. Khelil, Deep insights into the coupled optoelectronic analysis of ETL thin films and photovoltaic analysis of CsPbI3-based perovskite solar cell using SCAPS-1D simulations. Opt. Quantum Electron. **57**, 262 (2025). https://doi.org/10.1007/s11082-025-08200-5

Y. Ogomi, A. Morita, S. Tsukamoto, T. Saitho, N. Fujikawa, Q. Shen, T. Toyoda, K. Yoshino, S.S. Pandey, T. Ma, S. Hayase, CH 3 NH 3 Sn x Pb (1 –x) I 3 perovskite solar cells covering up to 1060 nm. J. Phys. Chem. Lett. **5**, 1004–1011 (2014). https://doi.org/10.1021/jz5002117

C.C.Stoumpos,C.D.Malliakas,M.G.Kanatzidis,Semiconductingtinandleadiodideperovskiteswithorganiccations:phasetransitions, highmobilities, and near-infrared photoluminescent properties. Inorg. Chem. **52**, 9019–9038 (2013). https://doi.org/10.1021/ic401215x

H.H. AbdelAziz, Performance evaluation of free hole-transport layer CsPbI3 perovskite solar cells. J. Mater. Sci. Mater. Electron. **34**, 470 (2023). https:// doi.org/10.1007/s10854-022-09624-5

E.M. Hutter, G.E. Eperon, S.D. Stranks, T.J. Savenije, Charge carriers in planar and meso-structured organic-inorganic perovskites: mobilities, lifetimes, and concentrations of trap states. J. Phys. Chem. Lett. **6**, 3082–3090 (2015). https://doi.org/10.1021/acs.jpclett.5b01361

H.-S. Kim, C.-R. Lee, J.-H. Im, K.-B. Lee, T. Moehl, A. Marchioro, S.-J. Moon, R. Humphry-Baker, J.-H. Yum, J.E. Moser, Lead iodide perovskite sensitized all-solid-state submicron thin film mesoscopic solar cell with efficiency exceeding 9%. Sci. Rep. **2**(1), 591 (2012)

M.M. Lee, J. Teuscher, T. Miyasaka, T.N. Murakami, H.J. Snaith, Efficient hybrid solar cells based on meso-superstructured organometal halide perovskites. Science **338**, 643–647 (2012)

W.S. Yang, B.-W. Park, E.H. Jung, N.J. Jeon, Y.C. Kim, D.U. Lee, S.S. Shin, J. Seo, E.K. Kim, J.H. Noh, Iodide management in formamidinium-leadhalide–based perovskite layers for efficient solar cells. Science **356**, 1376–1379 (2017)

W.E. Sha, X. Ren, L. Chen, W.C. Choy, The efficiency limit of CH3NH3PbI3 perovskite solar cells. Appl. Phys. Lett. (2015). https://doi.org/10.1063/ 1.4922150

J.M. Hoffman, I. Hadar, X. Li, W. Ke, E.S. Vasileiadou, J. Strzalka, L.X. Chen, M.G. Kanatzidis, Film formation mechanisms in mixed-dimensional 2D/3D halide perovskite films revealed by in situ grazing-incidence wide-angle X-ray scattering. Chem **8**(4), 1067–1082 (2022)

T.J. Millar, C. Walsh, M. Van de Sande, A.J. Markwick, The UMIST database for astrochemistry 2022, arXiv Preprint arXiv:2311.03936 (2023). https:// www.aanda.org/articles/aa/pdf/forth/aa46908-23.pdf (accessed January 21, 2024).

S.E. Boussaada, Y. Mouchaal, Performance Optimization of an Inorganic Lead-Free CsGeI3 Based Perovskite Solar Cells by SCAPS-1D Simulation. Arab. J. Sci. Eng. (2025). https://doi.org/10.1007/s13369-025-10517-y

A.K. Datta, M.K. Hossain, M.S. Rahman, P. Paramasivam, A. El-marghany, V.K. Mishra, DFT insights into bandgap engineering of lead-free LiMCl3 (M Mg, Be) halide perovskites for optoelectronic device applications. Sci. Rep. **15**, 6944 (2025). https://doi.org/10.1038/s41598-025-90621-z 26. M.A. Green, A. Ho-Baillie, H.J. Snaith, The emergence of perovskite solar cells. Nat. Photon. **8**, 506–514 (2014). https://doi.org/10.1038/nphoton.2014. 134

B. Padmaja, S. Dhanapandian, P. Paramasivam, A.G. Ayanie, Enhanced solar photocatalysis: vapor pressure synthesis of Ni-doped SnO2 nanoparticles for efficient organic dye degradation. ChemistrySelect **10**, e202500201 (2025). https://doi.org/10.1002/slct.202500201

VPMP Polytechnic, LDRP campus, Gandhinagar, K. Bhavsar, P.B. Lapsiwala, Sarvajanik College of Engineering and Technology, Surat Gujarat, India, Numerical simulation of perovskite solar cell with different material as electron transport layer using SCAPS-1D software. SPQEO **24**, 341–347 (2021). https://doi.org/10.15407/spqeo24.03.341

M.K. Assadi, S. Bakhoda, R. Saidur, H. Hanaei, Recent progress in perovskite solar cells. Renew. Sustain. Energy Rev. **81**, 2812–2822 (2018). https:// doi.org/10.1016/j.rser.2017.06.088

K. Zeghdar, S. Mansouri, L. Dehimi, F. Pezzimenti, M.H. Abdellattif, A.M.S. Alhuthali, C.J. Raorane, R. Balachandran, M.K. Hossain, Optimizing photovoltaic efficiency in CZTS solar cells by investigating the role of different advanced materials as back surface field layer. Sci. Rep. **15**, 25294 (2025). https://doi.org/10.1038/s41598-025-10958-3

W. Tress, N. Marinova, T. Moehl, S.M. Zakeeruddin, M.K. Nazeeruddin, M. Grätzel, Understanding the rate-dependent J-V hysteresis, slow time component, and aging in CH3NH3PbI3 perovskite solar cells: the role of a compensated electric field. Energy Environ. Sci. **8**, 995–1004 (2015). https:// doi.org/10.1039/C4EE03664F

P.K. Kanti, D. Jayan K, J. Swapnalin, P. Banerjee, P. Paramasivam, V.V. Wanatasanappan, A critical review on MXene as promising photovoltaic materials. Solar Energy Mater. Solar Cells **277**, 113147 (2024). https://doi.org/10.1016/j.solmat.2024.113147

A.M. Al-Hamdi, U. Rinner, M. Sillanpää, Tin dioxide as a photocatalyst for water treatment: a review. Process. Saf. Environ. Prot. **107**, 190–205 (2017). https://doi.org/10.1016/j.psep.2017.01.022

N. Rai, S. Rai, P.K. Singh, P. Lohia, D.K. Dwivedi, Analysis of various ETL materials for an efficient perovskite solar cell by numerical simulation. J. Mater. Sci. Mater. Electron. **31**, 16269–16280 (2020). https://doi.org/10.1007/s10854-020-04175-z

S.E. Boussaada, Y. Mouchaal, H. Riane, A. Khelil, An investigation of structural, electrical and optical properties of metal free-Zinc oxide thin films using spray pyrolysis sol-gel techniques. Egypt. J. Chem. (2024). https://doi.org/10.21608/ejchem.2024.266541.9265